Colloids and Surfaces A: Physicochem. Eng. Aspects 462 (2014) 124–130

Contents lists available at ScienceDirect

Colloids and Surfaces A: Physicochemical and Engineering Aspects

journal homepage: www.elsevier.com/locate/colsurfa

Surface complexation of fluoride at the activated nano-gibbsite water interface

Meththika Vithanage [a,*], Anushka Upamali Rajapaksha [a], M.S. Bootharaju [b], T. Pradeep [b]

[a] Chemical and Environmental Systems Modeling Research Group, Institute of Fundamental Studies, Hantana Road, Kandy 20000, Sri Lanka
[b] DST Unit of Nanoscience, Department of Chemistry, Indian Institute of Technology Madras, India

HIGHLIGHTS

- Heat activation converted crystalline nano-gibbsite to a poorly crystalline solid.
- Surface area increased enormously by heat activation from 50 to 399 m^2/g.
- F^- formed a monodentate mononuclear complex at activated GNP in low concentrations.
- Multilayer complex formation was confirmed by the isotherm modeling.

GRAPHICAL ABSTRACT

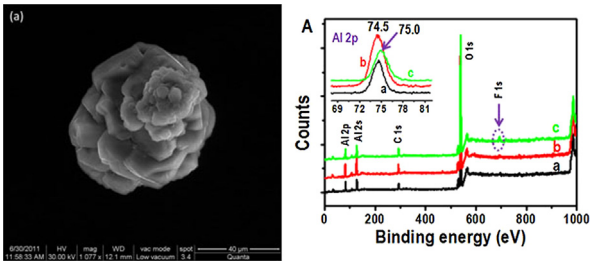

ARTICLE INFO

Article history:
Received 1 July 2014
Received in revised form 30 August 2014
Accepted 2 September 2014
Available online 16 September 2014

Keywords:
Gibbsite nanoparticles
Surface complexation modeling
X-ray photoelectron spectroscopy
Diffuse double layer

ABSTRACT

The drawbacks of existing fluoride removal processes are due to low efficiencies and less mechanistic understanding of the process. The acid–base protolysis and surface complexation constants for fluoride and thermally activated nanogibbsite were investigated in this study for the first time. Fluoride adsorption on heat activated gibbsite nanoparticles (HGNP) was determined as a function of pH, concentration of background electrolyte and adsorbate loading. XRD evidenced the HGNP is in a transient state of the formation of χ-alumina as a poorly crystalline solid. An immense increase in surface area was obtained from 50 to 399 m^2/g by the heat activation. Macroscopic data obtained from the batch experiments suggested an enhanced fluoride removal by HGNP with an adsorption maximum around pH 6. The adsorption quantified by the diffuse double layer surface complexation model indicated an inner sphere complexation mechanism at 0.526 mM of F^- with monodentate mononuclear complexes. An increase of fluoride concentration to 1.351 mM demonstrated a multilayer complex formation which was also confirmed by the isotherm data modeling with two distinct sorption maxima. XPS evidenced similar results showing two peaks at 684.7 and 688.5 eV for weak and strong bonded fluoride on HNGP surface. Fluoride adsorption maximum was reported as 4×10^{-6} mol/m^2 based on Langmuir data fitting.

1. Introduction

Toxic contaminants can be removed from aqueous solutions through interactions with solid phases present in the system. One of the most common interactions occurring between contaminants (sorbates) in solution and a solid phase (sorbent) is sorption. The term adsorption typically refers to the interaction of compounds on a solid surface, and absorption is related to accumulation in the internal region of a solid phase. Surface complexation is a thermodynamically based approach for describing adsorption in which solutes interact with functional groups on the surface either through ion pair association or solute-functional group complexation. Surface complexation models (SCMs) incorporate surface and aqueous complexation reactions as well as the electrical double

* Corresponding author. Tel.: +94 812232002; fax: +94 812232131.
E-mail address: meththikavithanage@gmail.com (M. Vithanage).

http://dx.doi.org/10.1016/j.colsurfa.2014.09.003
0927-7757/

layer theory (EDL) for describing metal adsorption onto mineral surfaces [1–5].

Fluoride is considered as the most reactive electronegative element of all the halides, and acquiring a great concern as a natural contaminant. In the natural environment, fluoride occurs as the fluoride ion, F^-. Fluorine, the element of fluoride, associates with many mineral deposits containing fluoride bearing minerals such as fluorite, apatite and mica. Weathering, dissolution and other pedogenic processes can release fluoride into groundwater even though fluoride is considered as an essential element for human health, especially for the strengthening of tooth enamel, excessive doses can be harmful [6]. Presence of fluoride in water does not impart any color, odor or taste. Therefore it acts as an invisible poison such as arsenic in groundwater. Among dental health concerns, dental fluorosis is the most common sign of excessive intake of fluoride rich drinking water. At the same time, low fluoride levels in the human body can lead to dental caries (decaying teeth and cavity formation). Severe chronic and cumulative over exposure can cause the incurable crippling of skeletal fluorosis (UNICEF, 2004). The dental or skeletal fluorosis is irreversible and no treatment exists. The presence of high fluoride in drinking water found in many parts of the world [7–11]. WHO [12] estimated that more than 260 million people worldwide consume drinking water with a fluoride content of >1.0 mg/L. Subsequently, a number of countries legislated to set 1.5 mg/L as the maximum contaminant level (MCL) for fluoride in drinking waters [13]. However, fluoride ingestion is from drinking and eating food cooked with fluoride rich water. Due to the climatic factors, people in tropics drink more water and the dosage could be exceeded. The majority of people live in tropical region where the problem is exacerbated by the need to drink more water because of the heat which exceeds the dosage.

Aluminum forms have shown a good affinity to fluoride ion [14,15]. However, most of the reported adsorption capacities are low [16,17], therefore new sorbents for fluoride removal is highly advantageous. The zirconium, iron and calcium oxide and magnesia nanoparticles showed an excellent ability to remove fluoride (F^-) from contaminated water over a wide range of pH [18–22]. However, not many have focused on alumina based nanoparticles for fluoride removal. Nanoparticles have unique adsorption properties due to their small size and large surface area, and hence in the present study, an attempt has been made to understand the fundamental interactions of gibbsite nanoparticle surface to fluoride in order to observe its potential to be a cheap and efficient adsorbent for fluoride removal. In this case, the SCMs play an important role as they are capable of simulating surface chemical reactions with a set of quasi thermodynamic constants which are independent of changes in solution conditions offering a distinct advantage over the often used conditional distribution coefficient, K_d [23]. Also, activation by heating may increase the potential of adsorption which may be effective in terms of pH of the working solutions and capacity. The application of SCMs on thermally activated nanogibbsite particles may provide acid–base protolysis and surface complexation constants for the first time. Hence, the application of SCM is useful to understand the interfacial interaction of fluoride on heated nanogibbsite. The present study deals with the mechanistic aspects of fluoride removal using activated gibbsite nanoparticles by heat treatment through batch experiments and SCMs.

2. Materials and methods

Gibbsite nanoparticles (GNPs) were prepared as the method given in Kumara et al. [24]. An amorphous aluminum hydroxide suspension obtained by a titration of $AlCl_3$ with NaOH around pH 4.6 was stirred thoroughly under nitrogen atmosphere. The suspension was dialyzed (Membrane D-9402 Sigma, USA), against distilled deionized water for 60 days maintaining the water phase and temperature at 50 °C until the chloride concentration was minimum. These GNPs were subjected to X-ray diffraction (XRD), and X-ray photoelectron spectroscopic (XPS) analyses before and after adsorption. Surface area was determined by the BET method. The surface titration was carried out to understand the surface charge of GNP using 1 g/L GNP with three different ionic strengths (0.001, 0.01 and 0.1 M $NaNO_3$). The suspension was equilibrated for 2 h prior to the titration with desired $NaNO_3$ concentration and N_2 gas was purged into the system throughout the titration to minimize CO_2 contamination. Point of zero charge (pH_{zpc}) of GNP was calculated based on the equilibrium H^+ and OH^-.

Acids, bases, and stock solutions were prepared in deionized and distilled waters. Precalibrated solutions of 0.1 M NaOH and 0.1 M HNO_3 were used for pH adjustments. Electrolytic concentration was regulated using 5.0 M $NaNO_3$. Analytical grade sodium fluoride (Fluka, Switzerland) was used for stock solutions. Fluoride analysis was carried out using an ion selective electrode with Thermo Orion 5 star multiparameter under CDTA-fluoride buffer, while aluminum also analyzed using atomic absorption spectrophotometer (GBC 933AA, Australia) for the samples to see any aluminum release into the solution. All the experiments were carried out in triplicates and the average values were presented in figures. The triplicates analysis were having good reproducibility with relative standard deviation of >10%.

2.1. Activation of gibbsite nanoparticles

Nano gibbsite samples were subjected to different heat treatment programs and analyzed for the fluoride adsorption as detailed above. For the heat treatment, 4 different temperatures were used, 300, 400, 800 and 1100 °C. Slow temperature increment was given for the GNP samples (7 °C/min), at the maximum temperature, GNP samples were kept for 3 h, and then allowed to drop to the room temperature slowly. Further, detailed batch experiments were conducted for the GNP with highest fluoride sorption. Heat treated GNP (HGNP from this point onwards) was undergone analysis for pH_{zpc}, BET, XRD and XPS.

2.2. Adsorption edges

Adsorption edges were obtained for three different ionic strengths having 100-fold variation (0.1, 0.01 and 0.001 M $NaNO_3$). Nano gibbsite suspension of 2 g/L was equilibrated overnight and spiked with fluoride to obtain a final concentration of 10 mg/L. Then the system pH was decremented to ~4.0 and incremented at ~0.5 pH intervals up to 9.5. At each point, a 10 mL sample portion was transferred into polypropylene tubes and equilibrated for 4 h at 100 rpm (EYELA B603 Shaker). Final pH of the suspension was recorded, membrane filtered (0.45 μm pore size) and directed to fluoride measurements with specific fluoride ion selective electrode (Orion 9409BN) with 1:1 CDTA buffer.

2.3. Adsorption isotherms

Loadings of fluoride were ranged from 0.263 to 3.947 mM for the adsorption isotherm study at 0.01 M $NaNO_3$. Similar to the edge experiments, 2 g/L suspension was hydrated for 2 h prior to the fluoride addition, equilibrated for 4 h, centrifuged and filtered for analysis. The pHs of the isotherm experiments were kept around 6.0. Data modeling was conducted using Langmuir (Eq. (1)) and Freundlich equations (Eq. (2)) respectively.

$$\Gamma = \Gamma_{Max} \frac{K_{ads}[A]}{1 + K_{ads}[A]} \quad (1)$$

Table 1
Properties of HGNP used in FITEQL optimization.

Parameter	Value	Reference
Surface area	399 m^2/g	This study
pH_{zpc} for HGNP	8.9	This study
Reactions		
$HF = H^+ + F^-$	3.18	Vithanage et al. [37]
$HF_2 = H^+ + 2F^-$	3.76	Vithanage et al. [37]

$$\Gamma = K_f[A]^{1/n} \quad (2)$$

where, Γ is fluoride adsorption per m^2 solid (mol/m^2), Γ_{max} is Langmuir constant associated with maximum adsorption capacity and K_{ads} is Langmuir equilibrium constant, A is equilibrium fluoride concentration, K_f and n are Freundlich constants representing the adsorption capacity and adsorption intensity, respectively.

2.4. Surface complexation modeling protocol

The potentiometric titration and adsorption edge data were interpreted by a surface complexation model in conjunction with a generalized diffuse double-layer model (DDLM) and 2-pK approach using the FITEQL computer algorithm [25]. The generalized DLM was selected due to its simplicity, applicability to different solution conditions, capability of handling several surface sites simultaneously, incorporation of high inner layer capacitance and low outer layer capacitance representation in a single surface layer of the DDLM and use of the Gouy–Chapman theory [1]. The 2-pK approach is widely used for metal (hydroxyl) oxides and in this case, the surface is hydroxylated in two steps:

$$\equiv AlOH + H^+ \rightarrow \equiv AlOH_2^+ \quad (3)$$

$$\equiv AlOH \rightarrow \equiv AlO^- + H^+ \quad (4)$$

The physicochemical data used for the SCM simulations are given in Table 1.

2.5. X-ray diffraction and photoelectron spectroscopic investigation

X-ray diffraction (XRD) analysis for the NGP, HGNP and fluoride loaded HGNP was performed by Shimadzu XD-D1 diffractometer using Cu Kα radiation (λ = 1.54 Å) radiation. Similarly, X-ray photoelectron spectroscopy (XPS) analyses were carried out for same samples. XPS measurements were conducted using Omicron ESCA Probe spectrometer with unmonochromatized Al Kα (energy = 1486.6 eV) X-rays. XPS spectra were calibrated by taking C 1s peak at 285.0 eV as an internal standard.

3. Results and discussion

3.1. Characteristics of GNP and activated GNP

Nano gibbsite used in this study showed a pH_{zpc} at 9.3 [24]. This pH_{zpc} value is in between the previous determinations of 9.1 [26], 9.6 [27] and 9.8 [28] for gibbsite. This difference in pH_{zpc} value is likely caused by the difference in synthesis [26]. We observed a decrease in the pH_{zpc} for 300 °C GNP and it may be due to the decrease in the electrostatic repulsion. Point of zero charge of the heat treated GNP at 300 °C was 8.85 (Fig. 1). Our findings for structural changes corroborate with Kumara et al. [24] and we hypothesized that these changes may influence the fluoride adsorption capacity of GNP. XRD data demonstrated the changes in the GNP structure (Fig. 2). The appearance of a sharp peak at 21.40° is ascribed to the development of the gibbsite phase along the (2 0 0) plane of gibbsite [24]. Characteristic peaks for gibbsite in 2-theta

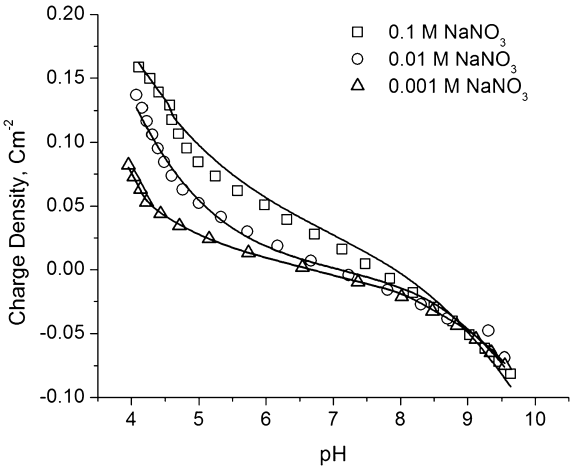

Fig. 1. Surface charge density (σ) of HGNP as a function of pH in different ionic strengths. Titrations were carried out under N_2 environment. Symbols represent the experimental data while solid lines representing DDLM model calculations.

degrees at 18.49, 20.52, 26.94, 36.90, 37.74, 40.28, 41.79, 44.49, 45.69, 50.92, 54.30 and 63.92 were resulted indicating formation of crystalline GNP. The XRD data of the heated GNP for 300 °C showed a transient phase between gibbsite and alumina [24]. Few characteristics peaks for χ-alumina [29] were observed in GNP heated at 300 °C (HGNP). The diffused XRD pattern expressed divergence of the crystalline nature of the GNP to amorphous structure (Fig. 2). The heated nano gibbsite at 300 °C evidenced the formation of χ-alumina (Fig. 2) as a poorly crystalline solid. X-ray diffractions of 37.4, 42.4, 47.4 and 67.1 HGNP can be assigned to the planes of (2 0 0), (2 0 2), (1 0 4) and (2 1 4) respectively, of χ-alumina [29].

Surface area of GNP showed a immense increase due to the heat treatment, especially in the case of HGNP at 300 °C (Table 1). BET surface area of GNP was found to be 50 m^2/g while it was increased to 399 m^2/g at 300 °C. This increase in BET surface area may be due to the transformation and recyrstalizing to a more thermodynamically stable phase due to the increase in temperature [30]. The changes of the surface from crystalline to amorphous nature and the changes in morphology were able to be observed by the SEM images as well (Fig. 3).

3.2. Adsorption vs. pH and ionic strength

Highest adsorption based on pH for GNP was observed around 2.5 mg/g (1.57×10^{-7} mol/m^2) for a sample spiked with 10 mg/L

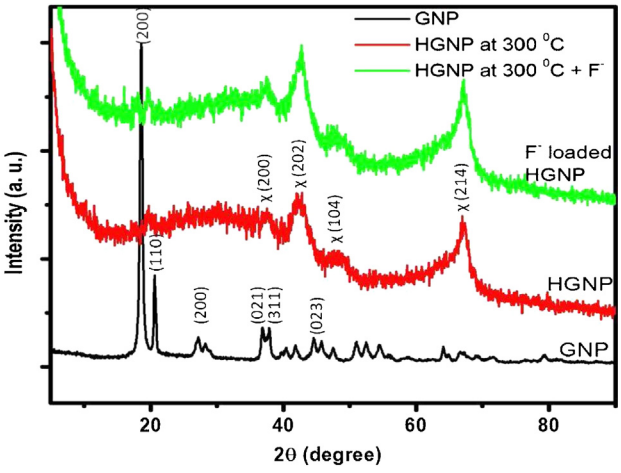

Fig. 2. X-ray diffraction spectra of GNP, HGNP and fluoride loaded HGNP.

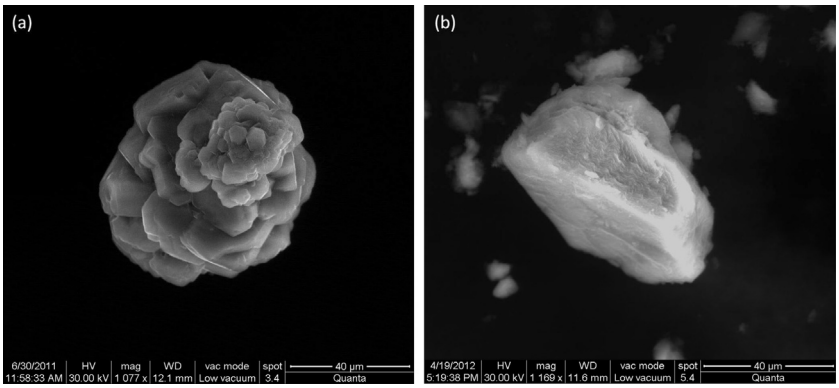

Fig. 3. Scanning electron microscopic images of GNP and HGNP showing the surface morphological changes in the synthesized and activated nanoparticles.

fluoride (data are not shown). However, the shape of the adsorption over a wide pH range (4–10), is almost parabolic. Maximum adsorption was in the pH range of 5–6.5. A considerable increase in adsorption was observed for the HGNP at 300 °C and the sorption remained same for the HGNP at 400 °C. Maximum adsorption of 5 mg/g (3.3×10^{-7} mol/m^2) was observed for HGNP. Note that the adsorption data exhibited a sharp increase in the fluoride sorption for the GNP heated upto 300 °C. However, further increase in temperature was not successful for increase in fluoride adsorption (data are not shown). Therefore, we limit the discussion to GNP heated to 300 °C. The parabolic adsorption pattern was common for each and every adsorption edge experiment with high fluoride loading of 25 mg/L (1.315 mM).

In the case of high fluoride loading of 1.315 mM, the adsorption capacity showed an increase up to 12 mg/g (7.91×10^{-7} mol/m^2). Only a slight decrease in the adsorption capacity by 0.02% was observed with the 2.5 times increase of the fluoride loading. However, the broad pH range of the maximum adsorption was narrowed down to 5.6–6.1.

Changing background electrolyte concentrations influence the adsorption in 4 different ways; (a) effect on the double layer thickness and competition between electrolyte anion and sorbate [23], (b) electrical charge at the surface, (c) potential at the surface and (d) speciation of sorbate [31]. Fluoride sorption showed no ionic strength dependency for the low fluoride loading (0.526 mM), however, a slight dependency was observed for the higher fluoride loading but it was restricted to the lowest pH range of the studied system. Less or no ionic strength dependency indirectly proposes an inner sphere complexation mechanism.

When the loading increases to 1.351 mM, an outer sphere complexation may possibly attributed forming an outer layer fluoride adsorption. This is further can be explained by the anion effect on adsorption into metal oxide surfaces [32,33]. This is due to the pH_{zpc} change as a result of the anion loading [32,34]. At the time of high fluoride in the HGNP suspension, HGNP surface is responding as a variable potential surface whereas in the case of low fluoride loading the surface respond as a variable charge surface. Application of higher loading of fluoride causes the changes in the surface charge and the potential [35]. Increasing ionic strength at this point decreased the absolute potential of the HGNP surface, create positive charge at the adsorbing plane, thus decreased fluoride adsorption at low pHs. Hence, at low pHs, where the adsorption is higher than high pHs, formation of multi layers may have cause the outer sphere complex formation which has been indicated by the ionic strength dependency of experimental data. At high pHs, the potential of the adsorbing plane become negative, the effect of ionic strength reversed, thus fluoride adsorption increased with increasing ionic strength. These observations suggest that, depending upon the pH, sorbate loading and electrolyte concentrations, fluoride is adsorbed providing evidence for both specific and non-specific adsorption.

3.3. Surface complexation modeling

Potentiometric titration data and modeling represent the HGNP surface charge is mainly controlled by H^+ and OH^- ions in the aqueous media. The titration data were obtained from pH 4–9 since extreme pH may lead in dissolution of HGNP [36]. The data indicated that the HGNP surface sites behave amphoterically based on the pH of the media. Experimentally obtained surface charge curves at different electrolyte concentrations cross at the net zero point charge (pH_{zpc} 8.9) corroborate with other studies on Al hydroxides [26]. The model fits well with the experimental data incorporating diffuse double layer in the model with one reactive site, ≡AlOH (Fig. 1).

The proton affinity constants and the site densities of ≡AlOH, protonated and deprotonated species were obtained by numerical optimization using FITEQL [25]. Based on the reaction 1 and 2, calculated intrinsic acidity constants and site densities are reported in Table 2. Intrinsic acidic constants and site densities were weighted averaged and tabulated [1]. Proton affinity constants resulted from the potentiometric data modeling were agreed with the literature [26].

Fluoride may form ≡AlF complexes due to the high reactivity of fluoride exchange with hydroxyl ions at the ≡Al surface sites [37]. The similar ionic potential of the two ions has made it possible to replace each other on the ≡Al surface. Multidentate complex formation was not considered in the modeling framework as in the previous studies [38–40]. Reason behind this is the high reactivity of fluoride ion and the incapability of DDLM to incorporate outer sphere surface complexes. Similar results have reported for fluoride adsorption on soils [41]. Considering the above factors, only the following reactions were considered in modeling fluoride interface interaction on HGNP for DDLM calculations. Thus the possible reactions of fluoride into HGNP are suggested via the ligand exchange mechanism of uncharged surface sites;

$$\equiv\text{AlOH} + \text{H}^+ + \text{F}^- \Rightarrow \equiv\text{Al-F} + \text{H}_2\text{O} \quad (5)$$

Modeling experimental data using the non-linear least square fitting model, FITEQL [25] showed good fit for the low fluoride loading (0.526 mM). The stability constants calculated are tabulated in Table 2. Simulations were performed incorporating monodentate mononuclear interaction of fluoride. However, in the case of high fluoride loading as observed from the experimental due to the outer sphere complex formation at low pHs the model did not show convergence. It is solely due to the incapability of the DDLM to track non-specific sorption. But, at with the increase of pH sorption changed into inner sphere showing no effect by the ionic

Table 2
Optimized FITEQL results from potentiometric titration and adsorption edges.

Parameter	0.1 M	0.01 M	0.001 M	Weighted mean[a]
Site density				
≡AlOH	2.283×10^{-3}	2.19×10^{-3}	9.007×10^{-4}	2.260×10^{-3}
≡AlOH + $H^+ \rightarrow AlOH_2^+$	7.815	7.786	7.722	7.768
≡AlOH → AlO^- + H^+	−9.107	−9.040	9.125	−9.101
Surface complexation reactions			0.526 mM	
Monodentate monouclear reactions				
≡AlOH + F^- + $H^+ \Leftrightarrow$ AlF + H_2O	17.19	16.54	16.53	16.74
			1.315 mM	
	8.350	8.351	8.343	8.347

[a] Weighted averages were calculated from $\log K = \Sigma wi\,(\log K)i$, where $wi = (1/\sigma \log K)i/(\Sigma(1/\sigma \log K)i)$, where $\sigma \log K$ is the standard deviation obtained from FITEQL calculations.

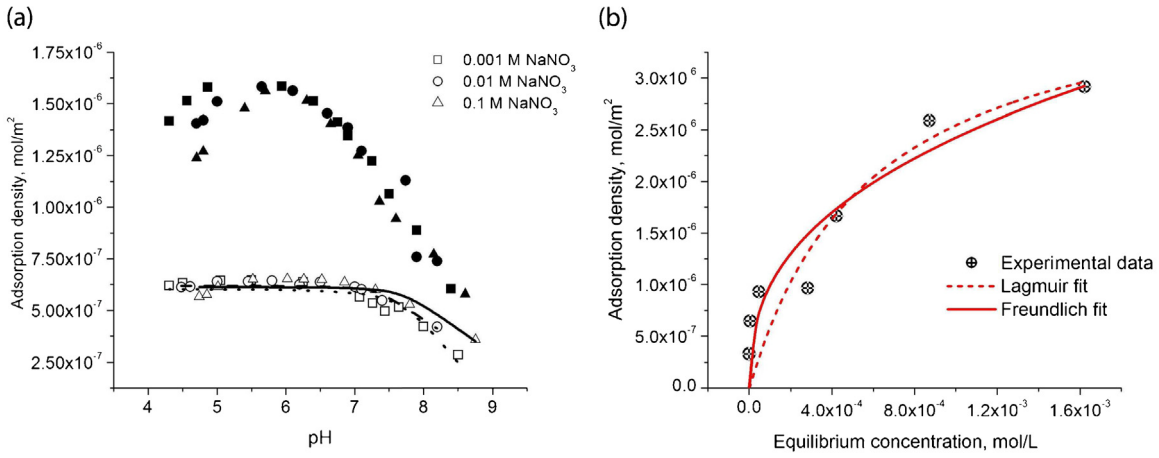

Fig. 4. Fluoride sorption edges (a) and isotherm data fitting for both Freundlich and Langmuir for HGNP (b). Open symbols at edge experimental data represent experimental data for low fluoride (0.526 mM) concentrations while closed symbols showed high fluoride loadings (1.315 mM) in three different ionic strengths. The experimental conditions used were: 2 g/L HGNP at temperature, 298 K.

strength showed a good fit with DDLM (Fig. 4a). Hence, it can be predicted that the strong HGNP – fluoride interaction mechanism as monodentate mononuclear whereas in the case of high fluoride concentrations it may form outer sphere weak bonding with HGNP surface.

3.4. Effect of fluoride loadings on heated nano gibbsite

Adsorption isotherms were conducted in order to understand the distribution of fluoride in HGNP and aqueous phase in the equilibrium. Adsorption behavior indicates fluoride sorption into microporous solid showing a L type shape of adsorption [42]. The interaction of fluoride is strong at low concentrations and with the increase of concentrations the pores and surfaces are filled with fluoride indicating a plateau reaching the monolayer coverage. This behavior indicates a typical chemisorptions behavior of surface interaction of species with the surface.

The data fitting obtained for both Langmuir and Freundlich isotherm equations (Eqs. (1) and (2)). Modeled data are given in Fig. 4b. Isotherm data fits well with Freundlich equation more than Langmuir fitting which implies multi layer adsorption of fluoride on HGNP surface. As it was observed by the adsorption edge results of 1.315 mM fluoride concentration, formation of outer sphere complexes at high fluoride concentration may have indicated by fitting the isotherm more to multi layer representing Freundlich isotherm.

Although the fitting was not as good as in the case of Freundlich, Langmuir data modeling showed a maximum adsorption density of 4.03×10^{-6} mol/m^2 which is equal to 30.55 mg/g of maximum fluoride adsorption. Compared to other studies, Γ_{max} of 30.55 mg/g remains quite high [43,44]. In Freundlich fitting, the slope or 1/n of an adsorption isotherm study is 0.39 (Table 3). Value below unity implies chemisorption as it is supported by the XPS data. The values for Freundlich constants and correlation coefficients (r^2) for the adsorption process are 4.00×10^{-5} mol/m^2 and 0.90 respectively.

3.5. XPS analysis

XPS studies have been carried out to understand the interaction between HNGP and F^- ions [14,15,45]. Comparison of survey spectra (Fig. 5A) of NGP, HNGP and HNGP + F^- samples confirms the presence of expected elements, Al and O. The presence of carbon is attributed to impurity which cannot be avoided. There is a new peak appeared in 680 eV region which is assigned to F in HNGP + F^- sample [46]. After F^- treatment, the Al 2p peak at 74.5 eV (in NGP and HNGP) is shifted to 75.0 eV which suggests the interaction of F^- with Al [47]. The specific regions of F, C and O are compared in Fig. 5B–D, respectively. The F 1s peaks observed at 684.7 and 688.5 eV are attributed to presence of F^- in two different chemical environments probably as physisorbed and chemisorbed fluoride species [48], respectively (Fig. 5B). The C 1s peaks are noticed at 285.0 eV attributed to aliphatic carbon impurities in all samples

Table 3
Isotherm constants for fluoride adsorption on HGNP at pH 6.0.

Freundlich	k_f ((mol/m^2)/(mol/dm^3)^n)	n	R^2	Chi^2
	4.00×10^{-5}	0.387	0.90	1.22×10^{-13}
Langmuir	Γ_{max} (mol/m^2)	K_L (dm^3 mol^{-1})	R^2	Chi^2
	4.03×10^{-6}	0.272	0.82	3.12×10^{-14}

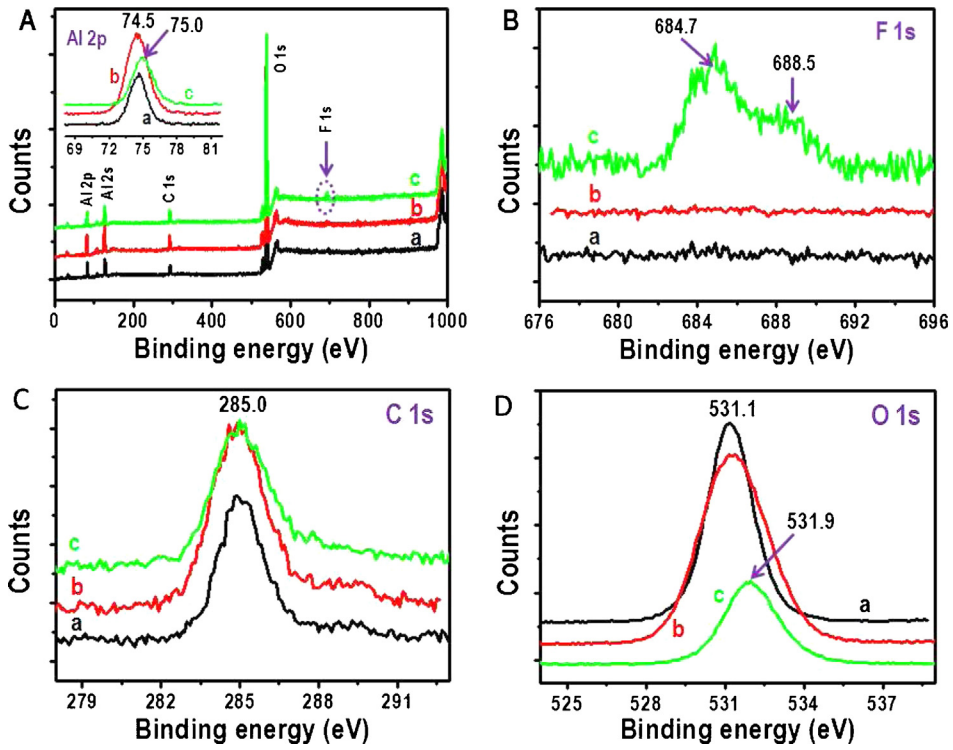

Fig. 5. XPS survey spectra (A) and expanded F 1s regions (B) of GNP, HGNP and F^- treated HGNP (traces a, b and c, respectively). Inset of A is Al 2p regions of samples a, b and c. C and D respectively are for C 1s and O 1s regions in same samples with fluoride loading of ~1.315 mM.

(Fig. 5C). There is shift of O 1s peak at 531.1 eV to 531.9 eV after treatment of F^- indicating the presence of F^- environment (Fig. 5D). From XPS analysis it is evident that F^- is interacting with Al of HNGP.

Dehydroxylation of gibbsite caused slight to moderate increases in its surface area as observed. Gibbsite heated to 300 °C had a microporous, granular appearance, consistent with surface area results. This structural transformation which has been attributed to the thermal treatment may have lead many Al sites to be available on the amorphous surface of χ-alumina due to the microporous structure. This may be the reason behind the increase in fluoride sorption which was observed clearly by the XPS and XRD data. Although an increase in surface sites occurred by the thermal treatment, the increase in sites may change with the holding time of the peak temperature and size of the gibbsite particles. Therefore, the prediction of the increase in sites may be difficult and condition specific.

4. Conclusions

Heated nano gibbsite at 300 °C indicated a phase transformation of the crystalline gibbsite nano particles into amorphous χ-gibbsite. This was evidenced by XRD and SEM data. Modeling data revealed that the increased surface area may have resulted high fluoride sorption capacity of 4×10^{-6} mol/m^2 which is equal to 39 mg/g from the HGNP. No pH or ionic strength dependency was observed in the pH range 4–6.5, suggesting an inner-sphere binding mechanism for low surface loads (0.526 mM). Surface titration and adsorption data were modeled well with DDLM. However, the fluoride adsorption was deviated from the monolayer to multi-layer when the initial loading was increased. The initial saturation of HGNP surface was attained at fluoride concentration of ~1.053 mM. These findings showed that the fluoride is efficiently adsorbed on HGNP surface forming monodentate mononuclear inner sphere complexes.

Acknowledgement

MV would like to thank Asanka Madhave Chandrasena for the assistance given during batch experiments.

References

[1] D.A. Dzombak, F.M.M. Morel, Surface Complexation Modeling – Hydorus Ferric Oxide, Wiley-Interscience, New York, 1990.
[2] K.F. Hayes, L.E. Katz, Application of X-ray absorption spectroscopy for surface complexation modeling of metal ion adsorption, in: P.V. Brady (Ed.), Physics and Chemistry of Mineral Surfaces, CRC Press, Boca Raton, FL, 1996, pp. 147–223.
[3] M. Vithanage, A.U. Rajapaksha, X. Dou, N.S. Bolan, J.E. Yang, Y.S. Ok, Surface complexation modeling and spectroscopic evidence of antimony adsorption on iron-oxide-rich red earth soils, J. Colloid Interface Sci. 406 (2013) 217–224.
[4] M. Kersten, S. Karabacheva, N. Vlasova, R. Branscheid, K. Schurk, H. Stanjek, Surface complexation modeling of arsenate adsorption by akagenéite (β-FeOOH)-dominant granular ferric hydroxide, Colloids Surf. Physicochem. Eng. Asp. 448 (2014) 73–80.
[5] Z. Wang, D.E. Giammar, Mass action expressions for bidentate adsorption in surface complexation modeling: theory and practice, Environ. Sci. Technol. 47 (2013) 3982–3996.
[6] C.B. Dissanayake, The fluoride problem in the groundwater of Sri Lanka – environmental management and health, Int. J. Environ. Stud. 38 (1991) 137–156.
[7] A.M. Abdelgawad, K. Watanabe, S. Takeuchi, T. Mizuno, The origin of fluoride-rich groundwater in Mizunami area, Japan – mineralogy and geochemistry implications, Eng. Geol. 108 (2009) 76–85.
[8] S. Ayoob, A.K. Gupta, Fluoride in drinking water: a review on the status and stress effects, Crit. Rev. Environ. Sci. Technol. 36 (2006) 433–487.
[9] C.B. Dissanayake, Water quality in the dry zone of Sri Lanka – some interesting health aspects, J. Natl. Sci. Found. Sri Lanka 33 (2005) 161–168.
[10] S. Cordeiro, R. Coutinho, J.V. Cruz, Fluoride content in drinking water supply in São Miguel volcanic island (Azores, Portugal), Sci. Total Environ. 432 (2012) 23–36.
[11] K. Brindha, L. Elango, Fluoride in groundwater: causes, implications and mitigation measures, in: S.D. Monroy (Ed.), Fluoride Properties, Applications and Environmental Management, 2011, pp. 111–136.
[12] WHO, Fluorine and fluorides, in: Environmental Health Criteria, World Health Organization, Geneva, Switzerland, 1984.
[13] WHO, Trace Elements in Human Nutrition and Health, World health Organization, Geneva, Switzerland, 1996.
[14] W. Zhang, M. Sun, R. Prins, Multinuclear MAS NMR identification of fluorine species on the surface of fluorinated γ-alumina, J. Phys. Chem. B. 106 (2002) 11805–11809.

[15] J.P. Nordin, D.J. Sullivan, B.L. Phillips, W.H. Casey, Mechanisms for fluoride-promoted dissolution of bayerite [β-$Al(OH)_3$(s)] and boehmite [γ-AlOOH]: ^{19}F-NMR spectroscopy and aqueous surface chemistry, Geochim. Cosmochim. Acta 63 (1999) 3513–3524.
[16] M. Mohapatra, S. Anand, B.K. Mishra, D.E. Giles, P. Singh, Review of fluoride removal from drinking water, J. Environ. Manage. 91 (2009) 67–77.
[17] P. Loganathan, S. Vigneswaran, J. Kandasamy, R. Naidu, Defluoridation of drinking water using adsorption processes, J. Hazard. Mater. 248–249 (2013) 1–19.
[18] S.M. Maliyekkal, K.R. Anshup, T. Antony, Pradeep, High yield combustion synthesis of nanomagnesia and its application for fluoride removal, Sci. Total Environ. 408 (2010) 2273–2282.
[19] X. Dou, Y. Zhang, H. Wang, T. Wang, Y. Wang, Performance of granular zirconium–iron oxide in the removal of fluoride from drinking water, Water Res. 45 (2011) 3571–3578.
[20] X. Zhao, J. Wang, F. Wu, T. Wang, Y. Cai, Y. Shi, G. Jiang, Removal of fluoride from aqueous media by Fe_3O_4@$Al(OH)_3$ magnetic nanoparticles, J. Hazard. Mater. 173 (2010) 102–109.
[21] P.K. Raul, R.R. Devi, I.M. Umlong, S. Banerjee, L. Singh, M. Purkait, Removal of fluoride from water using iron oxide-hydroxide nanoparticles, J. Nanosci. Nanotechnol. 12 (2012) 3922–3930.
[22] Y. Tang, X. Guan, J. Wang, N. Gao, M.R. McPhail, C.C. Chusuei, Fluoride adsorption onto granular ferric hydroxide: effects of ionic strength, pH, surface loading, and major co-existing anions, J. Hazard. Mater. 171 (2009) 774–779.
[23] K.F. Hayes, C. Papelis, J.O. Leckie, Modeling ionic strength effects on anion adsorption at hydrous oxide/solution interfaces, J. Colloid Interface Sci. 125 (1988) 717–726.
[24] C.K. Kumara, W.J. Ng, A. Bandara, R. Weerasooriya, Nanogibbsite: synthesis characterization, J. Colloid Interface Sci. 352 (2010) 252–258.
[25] A.L. Herbelin, J.C. Westall, FITEQL – A Computer Program for Determination of Chemical Equilibrium Constants from Experimental Data, Report 99-01, Department of Chemistry, Oregon State University, Corvallis, OR, 1999.
[26] S. Goldberg, Competitive adsorption of molybdenum in the presence of phosphorus or sulfur on gibbsite, Soil Sci. 175 (2010) 105–110.
[27] S. Goldberg, H.S. Forster, C.L. Godfrey, Molybdenum adsorption on oxides, clay minerals, and soils, Soil Sci. Soc. Am. J. 60 (1996) 425–432.
[28] B.A. Manning, S. Goldberg, Modeling competitive adsorption of arsenate with phosphate and molybdate on oxide minerals, Soil Sci. Soc. Am. J. 60 (1996) 121–131.
[29] Y. Liu, D. Ma, R.A. Blackley, W. Zhou, X. Han, X. Bao, Synthesis and characterization of gibbsite nanostructures, J. Phys. Chem. C. 112 (2008) 4124–4128.
[30] S. Goldberg, I. Lebron, D.L. Suarez, Z.R. Hinedi, Surface characterization of amorphous aluminum oxides contribution from the U.S. salinity lab, Soil Sci. Soc. Am. J. 65 (2001) 78–86.
[31] G.L. He, S.R. Cao, Assessment of fluoride removal from drinking water by calcium phosphate systems, Fluoride 29 (1996) 212–216.
[32] N.S. Bolan, N.J. Barrow, Modelling the effect of adsorption of phosphate and other anions on the surface charge of variable charge oxides, J. Soil Sci. 35 (1984) 273–281.
[33] R. Naidu, N.S. Bolan, R.S. Kookana, K.G. Tiller, Ionic-strength and pH effects on the sorption of cadmium and the surface charge of soils, Eur. J. Soil Sci. 45 (1994) 419–429.
[34] N.S. Bolan, J.K. Syers, R.W. Tillman, Ionic strength effects on surface charge and adsorption of phosphate and sulphate by soils, Eur. J. Soil Sci. 37 (1986) 379–388.
[35] L.M. He, L.W. Zelazny, V.C. Baligar, K.D. Ritchey, D.C. Martens, Ionic strength effects on sulfate and phosphate adsorption on gamma-alumina and kaolinite: triple-layer model, Soil Sci. Soc. Am. J. 61 (1997) 784–793.
[36] M. Vithanage, R. Chandrajith, A. Bandara, R. Weerasooriya, Mechanistic modeling of arsenic retention on natural red earth in simulated environmental systems, J. Colloid Interface Sci. 294 (2006) 265–272.
[37] M. Vithanage, L. Jayarathna, A.U. Rajapaksha, C.B. Dissanayake, M.S. Bootharaju, T. Pradeep, Modeling sorption of fluoride on to iron rich laterite, Colloids Surf. Physicochem. Eng. Asp. 398 (2012) 69–75.
[38] M.G. Sujana, H.K. Pradhan, S. Anand, Studies on sorption of some geomaterials for fluoride removal from aqueous solutions, J. Hazard. Mater. 161 (2009) 120–125.
[39] Y. Tang, J. Wang, N. Gao, Characteristics and model studies for fluoride and arsenic adsorption on goethite, J. Environ. Sci. 22 (2010) 1689–1694.
[40] X. Wu, Y. Zhang, X. Dou, M. Yang, Fluoride removal performance of a novel Fe–Al–Ce trimetal oxide adsorbent, Chemosphere 69 (2007) 1758–1764.
[41] G. Sposito, The Chemistry of Soils, Oxford University Press, New York, 1989.
[42] C.H. Giles, T.H. MacEwan, S.N. Nakhwa, D. Smith, Studies in adsorption. Part XI. A system of classification of solution adsorption isotherms, and its use in diagnosis of adsorption mechanisms and in measurement of specific surface areas of solids, J. Chem. Soc. 0 (1960) 3973–3993.
[43] S. Ayoob, A.K. Gupta, Insights into isotherm making in the sorptive removal of fluoride from drinking water, J. Hazard. Mater. 152 (2008) 976–985.
[44] A. Bhatnagar, E. Kumar, M. Sillanpää, Fluoride removal from water by adsorption—a review, Chem. Eng. J. 171 (2011) 811–840.
[45] J.D.A. Neville, Adsorption and Dissociation of Water and Hydrogen Fluoride Over the Surfaces of Aluminium Oxide Polymorphs, A Periodic Density Functional Theory Study, The University of Wales College of Cardiff (United Kingdom), Ann Arbor, 2004.
[46] H. Park, W. Choi, Effects of TiO_2 surface fluorination on photocatalytic reactions and photoelectrochemical behaviors, J. Phys. Chem. B. 108 (2004) 4086–4093.
[47] Y. Hua, Characterization of Binding Energy of Al Hexafluoride $[AlF_6]^{3-}$ in X-Ray Photoelectron Spectroscopy, in: 13th International Symposium on the Physical and Failure Analysis of Integrated Circuits, 2006, pp. 214–216.
[48] S. Yao, Y. Zheng, L. Ding, S. Ng, H. Yang, Co-promotion of fluorine and boron on $NiMo/Al_2O_3$ for hydrotreating light cycle oil, Catal. Sci. Technol. 2 (2012) 1925–1932.